

# The Mathematical Secret of Flight

Johan Hoffman<sup>a</sup> and Claes Johnson<sup>b</sup>

<sup>a</sup>Courant Institute, New York  
jhoffman@csc.kth.se

<sup>b</sup>School of Computer Science and Communication,  
Royal Institute of Technology, Stockholm  
cgjoh@kth.se

## 1 The Mystery of Flight

When you lean back for take-off in a jumbojet, maybe the following question flashes through your mind: How is it possible that the 400 squaremeter wings can carry 400 tons at a wingload of 1 ton per squaremeter in sustained flight in the air? Or maybe you are satisfied with some of the explanations offered in popular science, like higher velocity and lower pressure on the upper surface of the wing because it is curved and air there has a longer path to travel than below? Or maybe you are an aeroplane engineer or pilot and know very well why an airplane can fly?

In either case, you should get a bit worried by reading that the authority NASA on its website [43] dismisses all popular science theories for lift, including your favorite one, as being incorrect, but then refrains from presenting any theory claimed to be correct! NASA surprisingly ends with an empty out of reach: *To truly understand the details of the generation of lift, one has to have a good working knowledge of the Euler Equations.* The Plane&Pilot Magazine [44] has the same message and New York Times [8] informs us:

- *To those who fear flying, it is probably disconcerting that physicists and aeronautical engineers still passionately debate the fundamental issue underlying this endeavor: what keeps planes in the air?*

## 2 Overview

In this article we present a new mathematical and physical explanation of the generation of lift  $L$  and drag  $D$  of a wing based on new discoveries of the dynamics of *turbulent* air flow around a wing, obtained by computational solution of the basic mathematical model of fluid dynamics: the *Navier-Stokes/Euler equations*. When flying in the air, the downward gravitational force is balanced by upward wing lift  $L$ , while backward wing drag  $D$  is balanced by forward thrust from engine, and wing-beat for birds, or descent in gliding flight without forward thrust.

We show that a wing creates lift as a reaction force from redirecting air downwards, referred to as *downwash*, with less than 1/3 coming from the lower wing surface pushing

air down and the major remaining part from the upper surface sucking air down, with a resulting *lift/drag quotient*  $\frac{L}{D}$  of size 10 – 20.

The enigma of flight is why the air flow separates from the upper wing surface at the *trailing edge*, and not before, with the flow after separation being redirected downwards according to the tilting of the wing or *angle of attack*. We will reveal the secret to be an effect of a fortunate combination of features of *slightly viscous incompressible flow* including a crucial *instability mechanism at separation* analogous to that seen in the swirling flow down a bathtub drain, generating both suction on the upper wing surface and drag.

We show that this mechanism of lift and drag is operational for angles of attack smaller than a critical value of about 16 – 20 degrees depending on the shape of the wing, for which the flow separates from the upper wing surface well before the trailing edge with a sudden increase of drag and decrease of lift referred to as *stall*.

It is absolutely crucial that  $\frac{L}{D}$  is large, of size 10 or bigger, since otherwise the muscle power of a bird would not suffice, and the fuel consumption of an airplane would be prohibitive. Flying on a tilted barn door at 45 degrees angle of attack with  $\frac{L}{D} \approx 1$ , is not an option.

An outline of the article is as follows: We first recall classical theories for lift and drag and then in pictures describe the new theory. We support the new theory by computational solutions of the Navier-Stokes equations, also showing that the classical theories are incorrect. We then present basic aspects of the mathematics of *turbulent solutions of the Navier-Stokes equations* underlying the new theory.

### 3 Newton, d’Alembert and Kutta-Zhukovsky

The problem of explaining *why* it is possible to fly in the air using wings has haunted scientists since the birth of mathematical sciences. The mystery is *how* a sufficiently large ratio  $\frac{L}{D}$  can be created.

In the *gliding flight* of birds and airplanes with fixed wings at subsonic speeds,  $\frac{L}{D}$  is typically between 10 and 20, which means that a good glider can glide up to 20 meters upon loosing 1 meter in altitude, or that Charles Lindberg could cross the Atlantic in 1927 at a speed of 50 m/s in his 2000 kg *Spirit of St Louis* at an effective engine thrust of 150 kp (with  $\frac{L}{D} = 2000/150 \approx 13$ ) from 100 horse powers.

By Newton’s 3rd law, lift must be accompanied by downwash with the wing redirecting air downwards. The enigma of flight is the mechanism of a wing generating substantial downwash at small drag, which is also the enigma of sailing against the wind with both sail and keel acting like wings creating substantial lift [30].

Classical mathematical mechanics could not give an answer to the mystery of gliding flight: Newton computed by elementary mechanics the lift of a tilted flat plate redirecting a horizontal stream of fluid particles, but obtained a disappointingly small value proportional to the square of the angle of attack. To Newton the flight of birds was inexplicable, and human flight certainly impossible.

D’Alembert followed up in 1752 by formulating his paradox about zero lift/drag of *inviscid incompressible irrotational steady flow* referred to as *potential flow*, which seemed to describe the airflow around a wing since the viscosity of air is very small so that it can be viewed as being inviscid (with zero viscosity). Mathematically, potential flow is given as the gradient of a *harmonic function* satisfying *Laplace’s equation*.

At speeds less than say 300 km/h air flow is almost incompressible, and since a wing moves into still air the flow it could be expected to be irrotational without swirling rotating vortices. D'Alembert's mathematical potential flow thus seemed to capture physics, but nevertheless had neither lift nor drag, against all physical experience. The wonderful mathematics of potential flow and harmonic functions thus showed to be without physical relevance: This is *D'Alembert's paradox* which came to discredit mathematical fluid mechanics from start [26, 48, 7].

To explain flight d'Alembert's paradox had to be resolved, but nobody could figure out how and it was still an open problem when Orville and Wilbur Wright in 1903 showed that heavier-than-air human flight in fact was possible in practice, even if mathematically it was impossible.

Mathematical fluid mechanics was then saved from complete collapse by the young mathematicians Kutta and Zhukovsky, called the father of Russian aviation, who explained lift as a result of perturbing potential flow by a large-scale circulating flow or *circulation* around the two-dimensional section of a wing, and by the young physicist Prandtl, called the father of modern fluid dynamics, who explained drag as a result of a *viscous boundary layer* [45, 46, 47, 9].

This is the basis of state-of-the-art [16, 37, 14, 2, 19, 49, 50], which essentially is a simplistic theory for lift without drag at small angles of attack in inviscid flow and for drag without lift in viscous flow. However, state-of-the-art does not supply a theory for lift-and-drag covering the real case of *3d slightly viscous turbulent* flow of air around a 3d wing of a jumbojet at the critical phase of take-off at large angle of attack (12 degrees) and subsonic speed (270 km/hour), as evidenced in e.g. [1, 3, 4, 6, 8, 10, 34, 36, 41]. The simplistic theory allows an aeroplane engineer to roughly compute the lift of a wing a cruising speed at a small angle of attack, but not the drag, and not lift-and-drag at the critical phase of take-off [42, 13]. The lack of mathematics has to be compensated by experiment and experience. The first take off of the new Airbus 380 must have been a thrilling experience for the design engineers.

## 4 From Old to New Theory of Flight

A couple of years ago we stumbled upon a resolution of d'Alembert's paradox [25, 26], when computing turbulent solutions of the basic mathematical model of fluid mechanics, the Navier-Stokes equations. The resolution naturally led us to a new theory of flight, which we will explain below. You will find that it is quite easy to grasp, because it can be explained using different levels of mathematics. We start out easy with the basic principle in concept form and then indicate some of the mathematics with references to more details. Supporting information is given in the Google knols [32] and [33].

Before proceeding to work we recall both folklore and state-of-the-art mathematics explanations of flight as being either correct but trivial, or nontrivial but incorrect, as follows:

- Downwash generates lift: trivial without explanation of reason for downwash from suction on upper wing surface.
- Low pressure on upper surface: trivial without explanation why.
- Low pressure on curved upper surface because of higher velocity (by Bernouilli's law), because of longer distance: incorrect.

- Coanda effect: The flow sticks to the upper surface by viscosity: incorrect.
- Kutta-Zhukovsky: Lift comes from circulation: incorrect.
- Prandtl: Drag comes mainly from viscous boundary layer: incorrect.

## 5 The Principle of Flying

We will find that the secret of flight is revealed in Fig. 1: To the left we see potential flow around a portion of a long wing with zones of high (H) and low (L) pressure giving no net lift, because the pressure is high on top of the wing at the trailing edge and low below. This makes the flow leave the wing in the same direction as it approaches, thus without downwash and lift.

Potential flow is a mathematical solution without lift/downwash of the Navier-Stokes equations (with vanishing viscosity), which however is fundamentally different from the flow observed in reality with lift/downwash. Potential flow is a fictional mathematical solution without physical relevance, and the reason hides the secret of both d'Alembert's paradox and flight: Potential flow is very sensitive to a specific form of perturbation and thus is unstable and non-physical.

Potential flow is similar to an inverted pendulum in upright equilibrium or a pen balancing on its tip, which is a mathematical solution of the equations of motion, but an unstable non-physical solution which under a small perturbation away from the fully upright position will change into a different swinging motion. Potential flow without lift/downwash changes under a specific form of perturbation into a different more stable physical flow with lift/downwash, with a turbulent fluctuating layer including the perturbation attaching to the trailing edge, as we will see in computational simulations below with movies on [31].

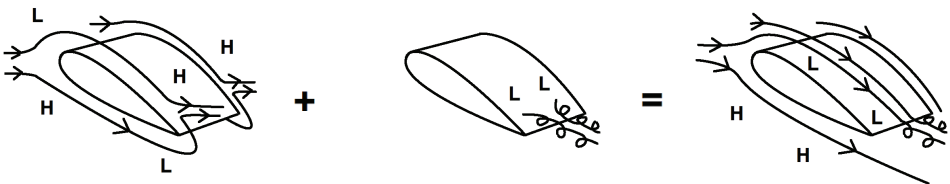


Figure 1: Correct explanation of lift by perturbation of potential flow (left) at separation from physical low-pressure turbulent counter-rotating rolls (middle) changing the pressure and velocity at the trailing edge into a flow with downwash and lift (right).

The specific form of perturbation is illustrated in the middle picture of Fig.1 showing a layer of counter-rotating rolls of swirling flow attaching to the trailing edge, with each roll similar to the swirling flow in a bathtub drain. The layer of rolls is distributed all along the trailing edge and is not related to the wing tip vortex, which often is seen at landing in moist air, since we assume the wing to be long. The perturbation switches the pressure distribution of potential flow at the trailing edge since the pressure inside the rolls is low, into the flow depicted to the right which has both lift, downwash and drag.

The specific perturbation thus hides the secret of flight as a flow with both lift, downwash and drag. By understanding mathematically the origin and nature of the instability

mechanism generating the counter-rotating rolls at the separation of potential flow, which we do in more detail below, we will be able to reveal the mathematical secret of flight. In short, the counterrotating rolls develop when the opposing flows from above and below meet on top of the wing before separation and first are retarded and then accelerated and stretched in the flow direction, as shown in detail in [25, 26, 24, 23]. We understand that inside the rolls of swirling flow the pressure must be low to keep the roll together, and it is this low pressure that annihilates the high pressure on top to allow the flow to leave the wing in the direction of the upper surface tangent with substantial downwash as illustrated in the figure.

We see that the fundamental instability mechanism changes the flow at the trailing edge to give lift, but does not change the flow at the leading edge where the flow gives positive lift. Real flow thus shares a very important property with potential flow, namely to not separate at the crest of the flow above the leading edge. If it did, downwash and lift would be lost: This is what happens when a wing stalls at a too large angle of attack.

Summing up we have that lift comes from the instability mechanism at separation consisting of counter-rotating low-pressure rolls of swirling flow, which also creates drag by suction from the low pressure. Thus lift comes along with drag: No lift without drag. Lift without drag is an illusion, although still a common dream.

## 6 Comparison with Kutta-Zhukovsky

We compare with the classical explanation presented by Kutta-Zhukovsky illustrated in Fig.2, which you find in most books claiming to explain flight: We see again potential flow, now around a section of the wing, but combined with a different perturbation consisting of large scale circulating flow around the wing. This perturbation also changes the pressure distribution to give lift/downwash as illustrated in the picture to the right. However, as we will see below, the circulating flow around the wing does not arise in reality: Kutta-Zhukovsky's circulating flow is purely fictional and generates lift/downwash by a non-physical mechanism which does not occur in reality.

Nevertheless, with no alternative in sight, Kutta-Zhukovsky's trick to generate downwash (lift) is generally viewed as a mathematically sophisticated way of explaining flight, beyond comprehension for most people. We shall find that the true reason it cannot be understood, is that it does not make sense, simply because there is no physical mechanism to generate the large scale circulation around the wing, nor the associated so-called *starting vortex* behind the wing supposedly balancing the circulation indicated in the right picture of Fig.2.

We observe that Kutta-Zhukovsky flow is two-dimensional, since both potential flow and circulation is constant in the wing direction and thus can be depicted in a plane figure, while the true flow is fully three-dimensional with the specific perturbation bringing in a variation in the wing direction. Kutta-Zhukovsky flow is like potential flow a non-physical two-dimensional stationary flow, while the real flow around a wing is a three-dimensional partially fluctuating turbulent flow.

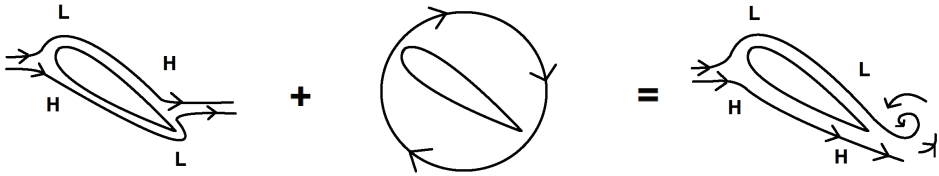


Figure 2: Incorrect Kutta-Zhukovsky explanation of lift by perturbation of potential flow (left) by unphysical circulation around the section (middle) resulting in flow with downwash/lift and starting vortex (right).

## 7 Effects of Small Viscosity

We conclude that flying is possible because of a fortunate combination of the following properties of real slightly viscous incompressible flow:

- non-separation at the crest of a wing because the flow is there similar to potential flow,
- the instability mechanism of potential flow at separation changes the pressure distribution at the trailing edge to give lift, and drag.

Slightly viscous flow has small *skin friction* along the boundary, which makes it similar to potential flow with zero skin friction satisfying a *slip* boundary condition at a solid boundary modeling that fluid particles can slide along the boundary without friction. Small skin friction can thus be modeled by zero skin friction requiring the normal velocity to vanish at the boundary, but imposing no restriction on the tangential velocity.

For a more viscous fluid like syrup with larger skin friction, instead a *no-slip* boundary condition is used requiring that both normal and tangential flow velocities vanish on the boundary modeling that fluid particles close to the boundary have small speed and connect to the interior flow by a *boundary layer* where the flow speed changes from zero to the free stream speed. The effect of a no-slip boundary condition causing a boundary layer, is that the flow separates at the crest with loss of lift as compared to slightly viscous flow. This is because in a viscous boundary layer the pressure gradient normal to the boundary vanishes and thus cannot contribute to the normal acceleration required to keep fluid particles following the curvature of the boundary after the crest, as shown in detail in [27]. It is thus the *slip boundary condition modeling a turbulent boundary layer* in slightly viscous flow, which forces the flow to suck to the upper surface and create downwash. Gliding flight in viscous flow is thus not possible, which explains why small insects do not practice gliding flight because to them air appears to be viscous.

## 8 Wellposedness vs Clay Millennium Problem

In order to judge the physical relevance of a mathematical solution, stability must be assessed. Only *wellposed* solutions which are suitably stable in the sense that small perturbations have small effects when properly measured, have physical significance as observable phenomena, as made clear by in particular the mathematician J. Hadamard in 1902

[15]. However, the completely crucial and fundamental question whether solutions of the Navier-Stokes equations are wellposed, has not been studied because of lack mathematical techniques for quantitative analysis, as evidenced in the formulation of the Clay Millennium Prize Problem on the Navier-Stokes equations excluding wellposedness [28, 24]. G. Birkhoff was heavily criticized for posing this question in [7], and refrained from further studies. The first step towards resolution of d'Alembert's paradox and the mathematical secret of flight is thus to pose the question if potential flow is wellposed, and then to realize that it is not. It took 256 years to take these steps.

## 9 Computed Lift and Drag

We now take a closer look at solutions of the Navier-Stokes equations, computed by the General Galerkin finite element method G2 [25]. These solutions should tell us the truth because the Navier-Stokes equations express the basic laws of physics of conservation of mass and momentum (Newton's 2nd law), which cannot be doubted. We focus on the case of slightly viscous incompressible flow of relevance for airplanes at subsonic speeds and larger birds. The fact that the fluid has small viscosity is of crucial importance both for physics and computation: First, the flow is then turbulent with a turbulent boundary layer allowing the flow to suck to the upper surface of the wing and cause downwash and lift. Second, a turbulent boundary layer can be modeled by a slip or small friction boundary condition which makes it possible to simulate the flow without computationally resolving thin boundary layers, which is impossible with any foreseeable computer [42].

We have indicated that the basic mechanism for the generation of lift of a wing consists of counter-rotating rolls of low-pressure *streamwise vorticity* (swirling flow) generated by instability at separation, which reduce the high pressure on top of the wing before the trailing edge of potential flow and thus allow downwash, but which also generate drag. At closer examination of the quantitative distributions of lift and drag forces around the wing, we discover large lift at the expense of small drag resulting from leading edge suction, which answers the opening question of how a wing can generate a lift/drag ratio larger than 10.

The secret of flight is in concise form uncovered in Fig. 3 showing G2 computed lift and drag coefficients of a Naca 0012 3d wing as functions of the angle of attack  $\alpha$ , as well as the circulation around the wing. We see that the lift and drag increase roughly linearly up to 16 degrees, with a lift/drag ratio of about 13 for  $\alpha > 3$  degrees, and that lift peaks at stall at  $\alpha = 20$  after a quick increase of drag. and flow separation at the leading edge.

We see that the circulation remains small for  $\alpha$  less than 10 degrees without connection to lift, and conclude that the theory of lift of by Kutta-Zhukovsky is fictional without physical correspondence: There is lift but no circulation. Lift does not originate from circulation. The incorrect explanation by Kutta-Zhukovsky is illustrated in Fig. 2 which is found in books on flight aerodynamics.

Inspecting Figs. 4-6 showing velocity, pressure and vorticity and Fig. 7 showing lift and drag distributions over the upper and lower surfaces of the wing (allowing also pitching moment to be computed), we can now, with experience from the above preparatory analysis, identify the basic mechanisms for the generation of lift and drag in incompressible slightly viscous flow around a wing at different angles of attack  $\alpha$ : We find two regimes

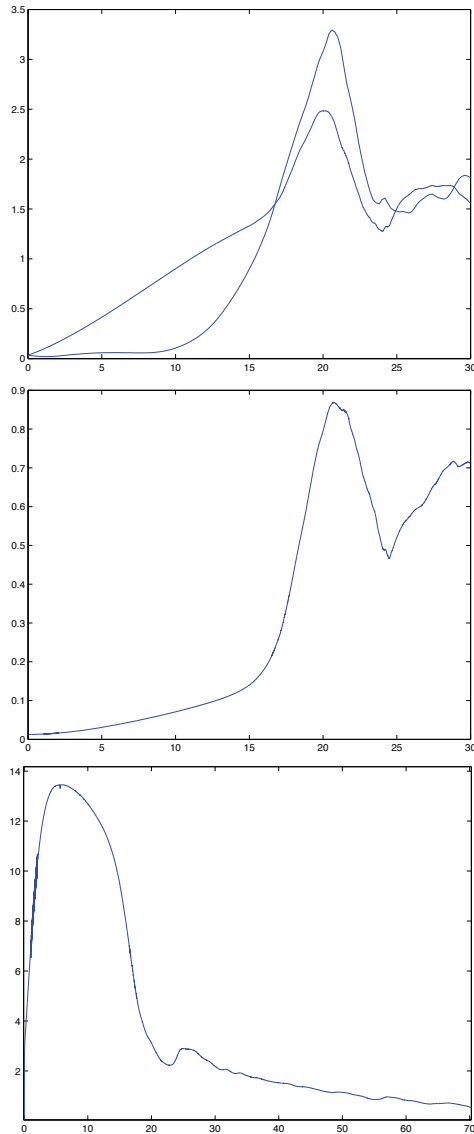


Figure 3: G2 lift coefficient and circulation as functions of the angle of attack (top), drag coefficient (middle) and lift/drag ratio (bottom) as functions of the angle of attack.

before stall at  $\alpha = 20$  with different, more or less linear growth in  $\alpha$  of both lift and drag, a main phase  $0 \leq \alpha < 16$  with the slope of the lift (coefficient) curve equal to 0.09 and of the drag curve equal to 0.008 with  $L/D \approx 14$ , and a final phase  $16 \leq \alpha < 20$  with increased slope of both lift and drag. The main phase can be divided into an initial phase  $0 \leq \alpha < 4 - 6$  and an intermediate phase  $4 - 6 \leq \alpha < 16$ , with somewhat smaller slope of drag in the initial phase. We now present details of this general picture.

### 10 Phase 1: $0 \leq \alpha \leq 4 - 6$

At zero angle of attack with zero lift there is high pressure at the leading edge and equal low pressures on the upper and lower crests of the wing because the flow is essentially potential and thus satisfies Bernouilli's law of high/low pressure where velocity is low/high. The drag is about 0.01 and results from rolls of low-pressure streamwise vorticity attaching to the trailing edge. As  $\alpha$  increases the low pressure below gets depleted as the incoming flow becomes parallel to the lower surface at the trailing edge for  $\alpha = 6$ , while the low pressure above intensifies and moves towards the leading edge. The streamwise vortices at the trailing edge essentially stay constant in strength but gradually shift attachment towards the upper surface. The high pressure at the leading edge moves somewhat down, but contributes little to lift. Drag increases only slowly because of negative drag at the leading edge.

### 11 Phase 2: $4 - 6 \leq \alpha \leq 16$

The low pressure on top of the leading edge intensifies to create a normal gradient preventing separation, and thus creates lift by suction peaking on top of the leading edge. The slip boundary condition prevents separation and downwash is created with the help of the low-pressure wake of streamwise vorticity at rear separation. The high pressure at the leading edge moves further down and the pressure below increases slowly, contributing to the main lift coming from suction above. The net drag from the upper surface is close to zero because of the negative drag at the leading edge, known as *leading edge suction*, while the drag from the lower surface increases (linearly) with the angle of the incoming flow, with somewhat increased but still small drag slope. This explains why the line to a flying kite can be almost vertical even in strong wind, and that a thick wing can have less drag than a thin.

### 12 Phase 3: $16 \leq \alpha \leq 20$

This is the phase creating maximal lift just before stall in which the wing partly acts as a bluff body with a turbulent low-pressure wake attaching at the rear upper surface, which contributes extra drag and lift, doubling the slope of the lift curve to give maximal lift  $\approx 2.5$  at  $\alpha = 20$  with rapid loss of lift after stall.

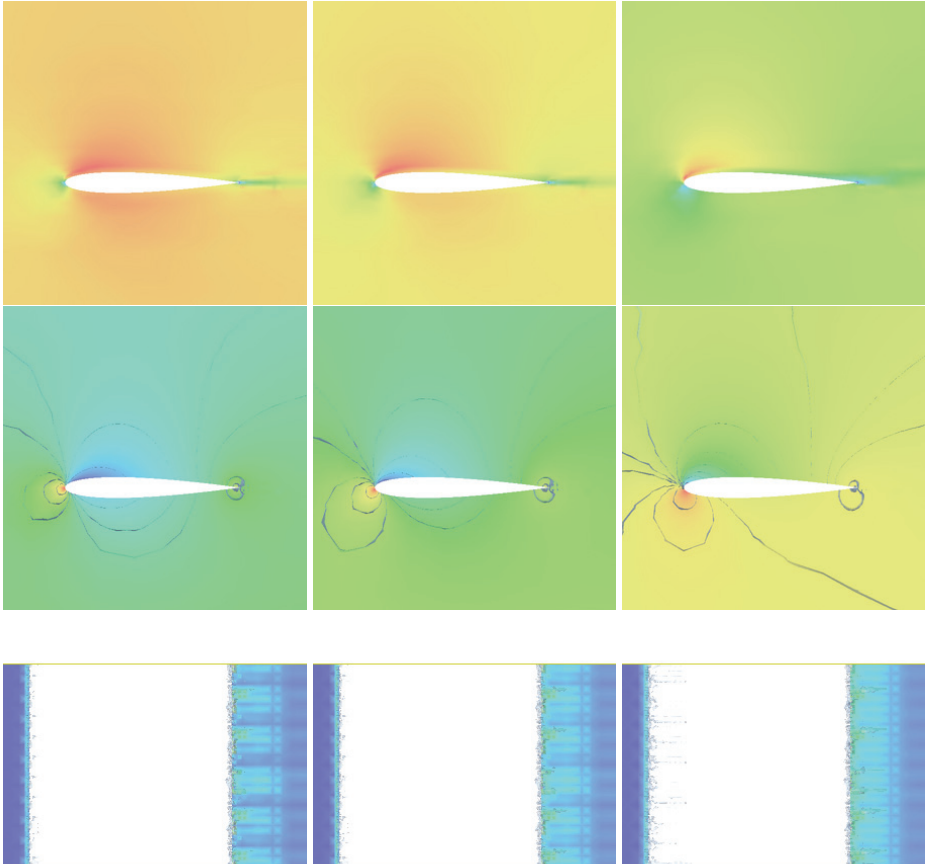


*Figure 4:* G2 computation of velocity magnitude (upper), pressure (middle), and non-transversal vorticity (lower), for angles of attack 2, 4, and  $8^\circ$  (from left to right). Notice in particular the rolls of streamwise vorticity at separation.

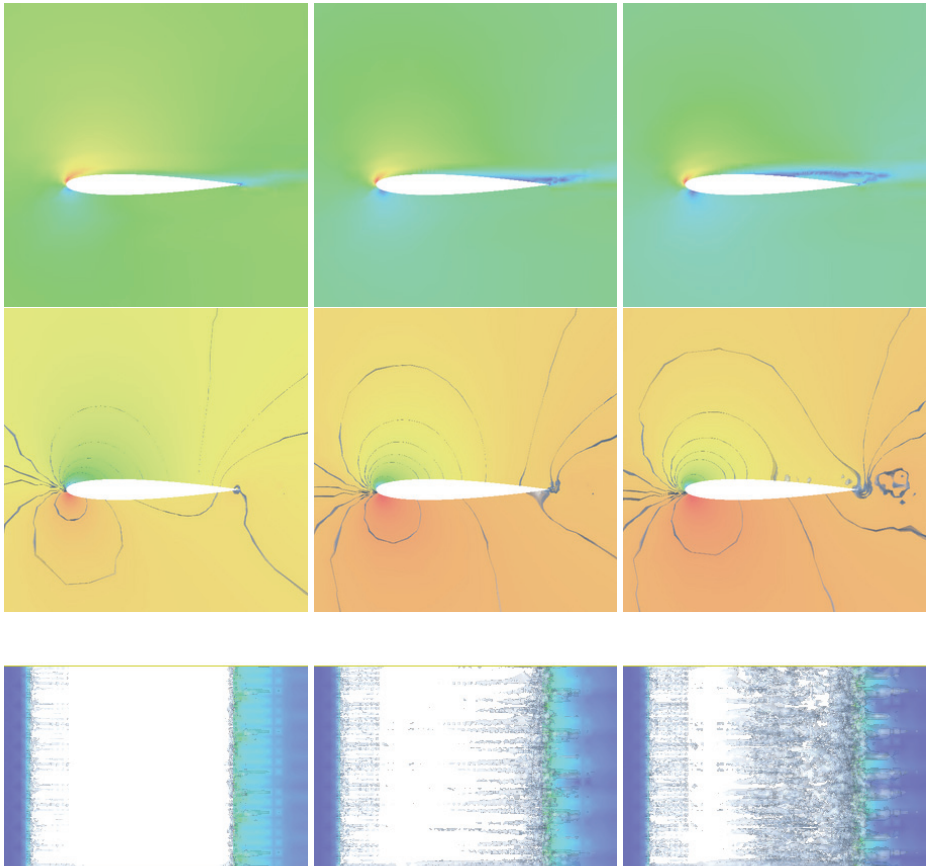


*Figure 5:* G2 computation of velocity magnitude (upper), pressure (middle), and topview of non-transversal vorticity (lower), for angles of attack 10, 14, and 18° (from left to right). Notice in particular the rolls of streamwise vorticity at separation.

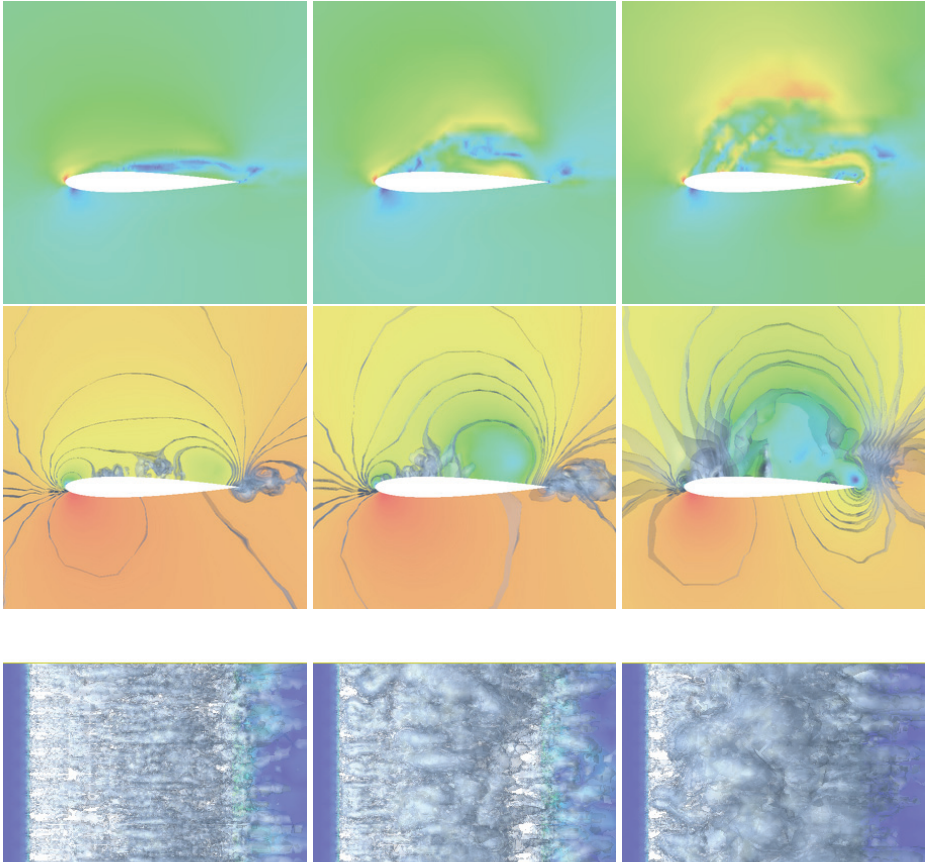


*Figure 6:* G2 computation of velocity magnitude (upper), pressure (middle), and non-transversal vorticity (lower), for angles of attack 20, 22, and 24° (from left to right).

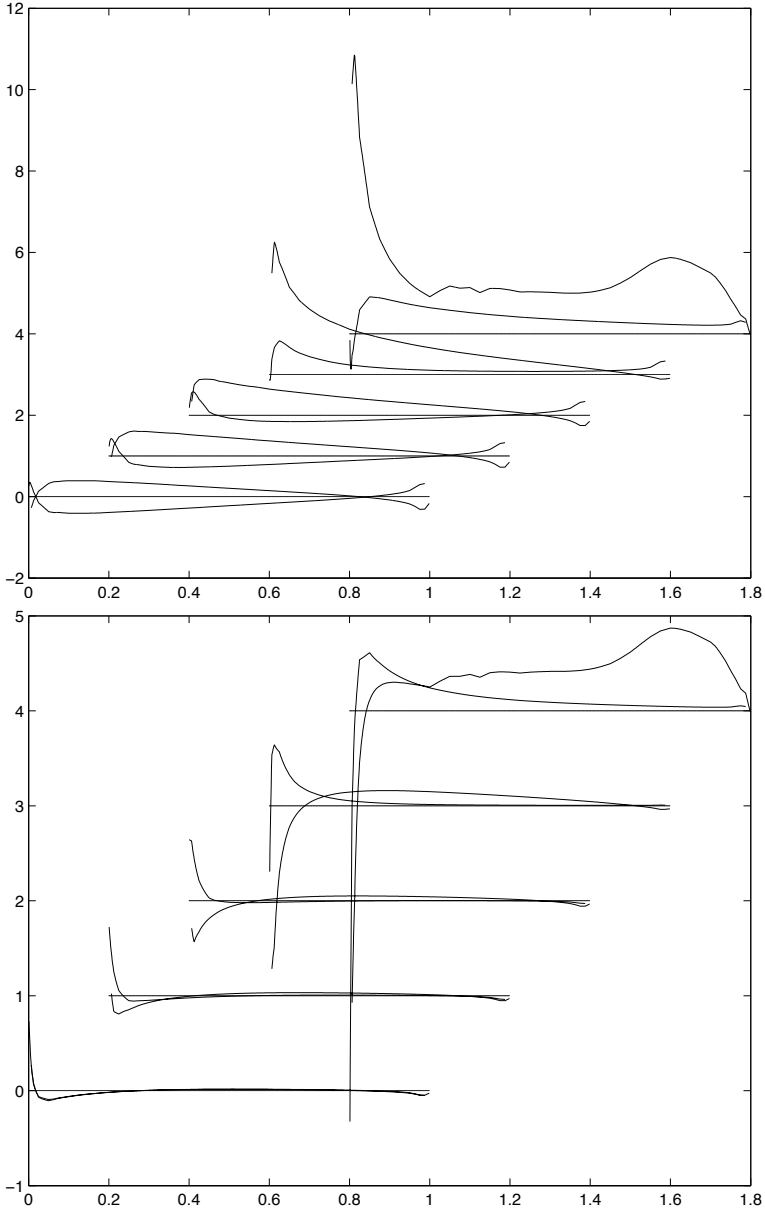


Figure 7: G2 computation of normalized local lift force (upper) and drag force (lower) contributions acting along the lower and upper parts of the wing, for angles of attack 0, 2, 4, 10 and 18°, each curve translated 0.2 to the right and 1.0 up, with the zero force level indicated for each curve.

### 13 Lift and Drag Distribution Curves

The distributions of lift and drag forces over the wing resulting from projecting the pressure acting perpendicular to the wing surface onto relevant directions, are plotted in Fig.7. The total lift and drag results from integrating these distributions around the wing. In potential flow computations (with circulation according to Kutta-Zhukovsky), only the pressure distribution or  $c_p$ -distribution is considered to carry relevant information, because a potential solution by construction has zero drag. In the perspective of Kutta-Zhukovsky, it is thus remarkable that the projected  $c_p$ -curves carry correct information for both lift and drag.

The lift generation in Phase 1 and 3 can rather easily be envisioned, while both the lift and drag in Phase 2 results from a (fortunate) intricate interplay of stability and instability of potential flow: The main lift comes from upper surface suction arising from a turbulent boundary layer with small skin friction combined with rear separation instability generating low-pressure streamwise vorticity, while the drag is kept small by negative drag from the leading edge.

### 14 Comparing Computation with Experiment

Comparing G2 computations with about 150 000 mesh points with experiments [20, 40], we find good agreement with the main difference that the boost of the lift coefficient in phase 3 is lacking in experiments. This is probably an effect of smaller Reynolds numbers in experiments, with a separation bubble forming on the leading edge reducing lift at high angles of attack. The oil-film pictures in [20] show surface vorticity generating streamwise vorticity in accordance with [24, 27, 23].

A jumbojet can only be tested in a wind tunnel as a smaller scale model, and upscaling test results is cumbersome because boundary layers do not scale. This means that computations can be closer to reality than wind tunnel experiments. Of particular importance is the maximal lift coefficient, which cannot be predicted by Kutta-Zhukovsky nor in model experiments, which for Boeing 737 is reported to be 2.73 in landing, corresponding to the maximal lift of 2.5 in computation for a long wing and not a full aircraft. In take-off the maximal lift is reported to be 1.75 with 1.5 in computation at a somewhat smaller angle of attack.

We compute turbulent solutions of the Navier-Stokes equations using a stabilized finite element method with *a posteriori* error control of lift and drag, referred to as *General Galerkin* or *G2*, available in executable open source from [17]. The stabilization in *G2* acts as an automatic turbulence model, and thus offers a model for *ab initio* computational simulation of the turbulent flow around a wing with the only input being the geometry of the wing. The computations performed on a single workstation show good agreement with experiments. We are now performing computations on super-computers allowing more precise comparisons and parameter studies.

## 15 Navier-Stokes with Force Boundary Conditions

For the reader interested in the mathematics we now present the Navier-Stokes equations along with a stability analysis exhibiting the basic instability mechanism at separation which is crucial for the generation of lift, at the expense of some drag.

The Navier-Stokes equations for an incompressible fluid of unit density with *small viscosity*  $\nu > 0$  and *small skin friction*  $\beta \geq 0$  filling a volume  $\Omega$  in  $\mathbb{R}^3$  surrounding a solid body with boundary  $\Gamma$  over a time interval  $I = [0, T]$ , read as follows: Find the velocity  $u = (u_1, u_2, u_3)$  and pressure  $p$  depending on  $(x, t) \in \Omega \cup \Gamma \times I$ , such that

$$\begin{aligned} \dot{u} + (u \cdot \nabla)u + \nabla p - \nabla \cdot \sigma &= f && \text{in } \Omega \times I, \\ \nabla \cdot u &= 0 && \text{in } \Omega \times I, \\ u_n &= g && \text{on } \Gamma \times I, \\ \sigma_s &= \beta u_s && \text{on } \Gamma \times I, \\ u(\cdot, 0) &= u^0 && \text{in } \Omega, \end{aligned} \tag{1}$$

where  $u_n$  is the fluid velocity normal to  $\Gamma$ ,  $u_s$  is the tangential velocity,  $\sigma = 2\nu\epsilon(u)$  is the viscous (shear) stress with  $\epsilon(u)$  the usual velocity strain,  $\sigma_s$  is the tangential stress,  $f$  is a given volume force,  $g$  is a given inflow/outflow velocity with  $g = 0$  on a non-penetrable boundary, and  $u^0$  is a given initial condition. We notice the skin friction boundary condition coupling the tangential stress  $\sigma_s$  to the tangential velocity  $u_s$  with the friction coefficient  $\beta$  with  $\beta = 0$  for slip, and  $\beta \gg 1$  for no-slip. We note that  $\beta$  is related to the standard *skin friction coefficient*  $c_f = \frac{2\tau}{U^2}$  with  $\tau$  the tangential stress per unit area, by the relation  $\beta = \frac{U}{2}c_f$ . In particular,  $\beta$  tends to zero with  $c_f$  (if  $U$  stays bounded).

Prandtl insisted on using a no-slip velocity boundary condition with  $u_s = 0$  on  $\Gamma$ , because his resolution of d'Alembert's paradox hinged on discriminating potential flow by this condition. On the other hand, with the new resolution of d'Alembert's paradox, relying instead on instability of potential flow, we are free to choose instead a friction force boundary condition, if data is available. Now, experiments show [47, 11] that the skin friction coefficient decreases with increasing Reynolds number  $Re$  as  $c_f \sim Re^{-0.2}$ , so that  $c_f \approx 0.0005$  for  $Re = 10^{10}$  and  $c_f \approx 0.007$  for  $Re = 10^5$ . Accordingly we model a turbulent boundary layer by a friction boundary condition with a friction parameter  $\beta \approx 0.03URe^{-0.2}$ . For very large Reynolds numbers, we can effectively use  $\beta = 0$  in G2 computation corresponding to slip boundary conditions.

As developed in more detail in [27], we make a distinction between laminar (boundary layer) separation modeled by no-slip and turbulent (boundary layer) separation modeled by slip/small friction. Note that laminar separation cannot be modeled by slip, since a laminar boundary layer needs to be resolved with no-slip to get correct (early) separation. On the other hand, as will be seen below, in turbulent (but not in laminar) flow the interior turbulence dominates the skin friction turbulence indicating that the effect of a turbulent boundary layer can be modeled by slip/small friction, which can be justified by an a posteriori sensitivity analysis as shown in [27].

We thus assume that the boundary layer is turbulent and is modeled by slip/small friction, which effectively includes the case of laminar separation followed by reattachment into a turbulent boundary layer.

## 16 Potential Flow

Potential flow  $(u, p)$  with velocity  $u = \nabla\varphi$ , where  $\varphi$  is harmonic in  $\Omega$  and satisfies a homogeneous Neumann condition on  $\Gamma$  and suitable conditions at infinity, can be seen as a solution of the Navier-Stokes equations for slightly viscous flow with slip boundary condition, subject to

- perturbation of the volume force  $f = 0$  in the form of  $\sigma = \nabla \cdot (2\nu\epsilon(u))$ ,
- perturbation of zero friction in the form of  $\sigma_s = 2\nu\epsilon(u)_s$ ,

with both perturbations being small because  $\nu$  is small and a potential flow velocity  $u$  is smooth. Potential flow can thus be seen as a solution of the Navier-Stokes equations with small force perturbations tending to zero with the viscosity. We can thus express d'Alembert's paradox as the zero lift/drag of a Navier-Stokes solution in the form of a potential solution, and resolve the paradox by realizing that potential flow is unstable and thus cannot be observed as a physical flow.

Potential flow is like an inverted pendulum, which cannot be observed in reality because it is unstable and under infinitesimal perturbations turns into a swinging motion. A stationary inverted pendulum is a fictitious mathematical solution without physical correspondence because it is unstable. You can only observe phenomena which in some sense are stable, and an inverted pendulum or potential flow is not stable in any sense.

Potential flow has the following crucial property which partly will be inherited by real turbulent flow, and which explains why a flow over a wing subject to small skin friction can avoid separating at the crest and thus generate downwash, unlike viscous flow with no-slip, which separates at the crest without downwash. We will conclude that gliding flight is possible only in slightly viscous incompressible flow. For simplicity we consider two-dimensional potential flow around a cylindrical body such as a long wing (or cylinder).

**Theorem.** Let  $\varphi$  be harmonic in the domain  $\Omega$  in the plane and satisfy a homogeneous Neumann condition on the smooth boundary  $\Gamma$  of  $\Omega$ . Then the streamlines of the corresponding velocity  $u = \nabla\varphi$  can only separate from  $\Gamma$  at a point of stagnation with  $u = \nabla\varphi = 0$ .

**Proof.** Let  $\psi$  be a harmonic conjugate to  $\varphi$  with the pair  $(\varphi, \psi)$  satisfying the Cauchy-Riemann equations (locally) in  $\Omega$ . Then the level lines of  $\psi$  are the streamlines of  $\varphi$  and vice versa. This means that as long as  $\nabla\varphi \neq 0$ , the boundary curve  $\Gamma$  will be a streamline of  $u$  and thus fluid particles cannot separate from  $\Gamma$  in bounded time.

## 17 Exponential Instability

Subtracting the NS equations with  $\beta = 0$  for two solutions  $(u, p, \sigma)$  and  $(\bar{u}, \bar{p}, \bar{\sigma})$  with corresponding (slightly) different data, we obtain the following linearized equation for the difference  $(v, q, \tau) \equiv (u - \bar{u}, p - \bar{p}, \sigma - \bar{\sigma})$  with :

$$\begin{aligned}
 \dot{v} + (u \cdot \nabla)v + (v \cdot \nabla)\bar{u} + \nabla q - \nabla \cdot \tau &= f - \bar{f} && \text{in } \Omega \times I, \\
 \nabla \cdot v &= 0 && \text{in } \Omega \times I, \\
 v \cdot n &= g - \bar{g} && \text{on } \Gamma \times I, \\
 \tau_s &= 0 && \text{on } \Gamma \times I, \\
 v(\cdot, 0) &= u^0 - \bar{u}^0 && \text{in } \Omega,
 \end{aligned} \tag{2}$$

Formally, with  $u$  and  $\bar{u}$  given, this is a linear convection-reaction-diffusion problem for  $(v, q, \tau)$  with the reaction term given by the  $3 \times 3$  matrix  $\nabla \bar{u}$  being the main term of concern for stability. By the incompressibility, the trace of  $\nabla \bar{u}$  is zero, which shows that in general  $\nabla \bar{u}$  has eigenvalues with real value of both signs, of the size of  $|\nabla \bar{u}|$  (with  $|\cdot|$  some matrix norm), thus with at least one exponentially unstable eigenvalue.

Accordingly, we expect local exponential perturbation growth of size  $\exp(|\nabla u|t)$  of a solution  $(u, p, \sigma)$ , in particular we expect a potential solution to be illposed. This is seen in G2 solutions with slip initiated as potential flow, which subject to residual perturbations of mesh size  $h$ , in  $\log(1/h)$  time develop into turbulent solutions. We give computational evidence that these turbulent solutions are wellposed, which we rationalize by cancellation effects in the linearized problem, which has rapidly oscillating coefficients when linearized at a turbulent solution.

Formally applying the curl operator  $\nabla \times$  to the momentum equation of (1), with  $\nu = \beta = 0$  for simplicity, we obtain the *vorticity equation*

$$\dot{\omega} + (u \cdot \nabla)\omega - (\omega \cdot \nabla)u = \nabla \times f \quad \text{in } \Omega, \tag{3}$$

which is a convection-reaction equation in the vorticity  $\omega = \nabla \times u$  with coefficients depending on  $u$ , of the same form as the linearized equation (2), with similar properties of exponential perturbation growth  $\exp(|\nabla u|t)$  referred to as *vortex stretching*. Kelvin's theorem formally follows from this equation assuming the initial vorticity is zero and  $\nabla \times f = 0$  (and  $g = 0$ ), but exponential perturbation growth makes this conclusion physically incorrect: We will see below that large vorticity can develop from irrotational potential flow even with slip boundary conditions.

### 18 Energy Estimate with Turbulent Dissipation

The standard *energy estimate* for (1) is obtained by multiplying the momentum equation

$$\dot{u} + (u \cdot \nabla)u + \nabla p - \nabla \cdot \sigma - f = 0,$$

with  $u$  and integrating in space and time, to get in the case  $f = 0$  and  $g = 0$ ,

$$\int_0^t \int_{\Omega} R_{\nu}(u, p) \cdot u \, dxdt = D_{\nu}(u; t) + B_{\beta}(u; t) \tag{4}$$

where

$$R_{\nu}(u, p) = \dot{u} + (u \cdot \nabla)u + \nabla p$$

is the *Euler residual* for a given solution  $(u, p)$  with  $\nu > 0$ ,

$$D_{\nu}(u; t) = \int_0^t \int_{\Omega} \nu |\epsilon(u(\bar{t}, x))|^2 \, dx d\bar{t}$$

is the *internal turbulent viscous dissipation*, and

$$B_{\beta}(u; t) = \int_0^t \int_{\Gamma} \beta |u_s(\bar{t}, x)|^2 \, dx d\bar{t}$$

is the *boundary turbulent viscous dissipation*, from which follows by standard manipulations of the left hand side of (4),

$$K_\nu(u; t) + D_\nu(u; t) + B_\beta(u; t) = K(u^0), \quad t > 0, \quad (5)$$

where

$$K_\nu(u; t) = \frac{1}{2} \int_\Omega |u(t, x)|^2 dx.$$

This estimate shows a balance of the *kinetic energy*  $K(u; t)$  and the *turbulent viscous dissipation*  $D_\nu(u; t) + B_\beta(u; t)$ , with any loss in kinetic energy appearing as viscous dissipation, and vice versa. In particular,

$$D_\nu(u; t) + B_\beta(u; t) \leq K(u^0),$$

and thus the viscous dissipation is bounded (if  $f = 0$  and  $g = 0$ ).

*Turbulent solutions* of (1) are characterized by *substantial internal turbulent dissipation*, that is (for  $t$  bounded away from zero),

$$D(t) \equiv \lim_{\nu \rightarrow 0} D(u_\nu; t) \gg 0, \quad (6)$$

which is *Kolmogorov's conjecture* [18]. On the other hand, the *skin friction dissipation* decreases with decreasing friction

$$\lim_{\nu \rightarrow 0} B_\beta(u; t) = 0, \quad (7)$$

since  $\beta \sim \nu^{0.2}$  tends to zero with the viscosity  $\nu$  and the tangential velocity  $u_s$  approaches the (bounded) free-stream velocity. We thus find evidence that the interior turbulent dissipation dominates the skin friction dissipation, which supports the use of slip as a model of a turbulent boundary layer, but which is not in accordance with Prandtl's (unproven) conjecture that substantial drag and turbulent dissipation originates from the boundary layer.

Kolmogorov's conjecture (6) is consistent with

$$\|\nabla u\|_0 \sim \frac{1}{\sqrt{\nu}}, \quad \|R_\nu(u, p)\|_0 \sim \frac{1}{\sqrt{\nu}}, \quad (8)$$

where  $\|\cdot\|_0$  denotes the  $L_2(Q)$ -norm with  $Q = \Omega \times I$ . On the other hand, it follows by standard arguments from (5) that

$$\|R_\nu(u, p)\|_{-1} \leq \sqrt{\nu}, \quad (9)$$

where  $\|\cdot\|_{-1}$  is the norm in  $L_2(I; H^{-1}(\Omega))$ . Kolmogorov thus conjectures that the Euler residual  $R_\nu(u, p)$  for small  $\nu$  is strongly (in  $L_2$ ) large, while being small weakly (in  $H^{-1}$ ).

Altogether, we understand that the resolution of d'Alembert's paradox of explaining substantial drag from vanishing viscosity, consists of realizing that the internal turbulent dissipation  $D$  can be positive under vanishing viscosity, while the skin friction dissipation  $B$  will vanish. In contradiction to Prandtl, we conclude that drag does not result from boundary layer effects, but from internal turbulent dissipation, originating from instability at separation.

## 19 G2 Computational Solution

We show in [25, 24, 26] that the Navier-Stokes equations (1) can be solved by G2 producing turbulent solutions characterized by substantial turbulent dissipation from the least squares stabilization acting as an automatic turbulence model, reflecting that the Euler residual cannot be made pointwise small in turbulent regions. G2 has a posteriori error control based on duality and shows output uniqueness in mean-values such as lift and drag [25, 21, 22]

We find that G2 with slip is capable of modeling slightly viscous turbulent flow with  $Re > 10^6$  of relevance in many applications in aero/hydro dynamics, including flying, sailing, boating and car racing, with hundred thousands of mesh points in simple geometry and millions in complex geometry, while according to state-of-the-art quadrillions is required [42]. This is because a friction-force/slip boundary condition can model a turbulent boundary layer, and interior turbulence does not have to be resolved to physical scales to capture mean-value outputs [25].

The idea of circumventing boundary layer resolution by relaxing no-slip boundary conditions introduced in [21, 25], was used in [39, 5] in the form of weak satisfaction of no-slip, which however misses the main point of using a force condition instead of a velocity condition in a model of a turbulent boundary layer.

A G2 solution  $(U, P)$  on a mesh with local mesh size  $h(x, t)$  according to [25], satisfies the following energy estimate (with  $f = 0, g = 0$  and  $\beta = 0$ ):

$$K(U(t)) + D_h(U; t) = K(u^0), \tag{10}$$

where

$$D_h(U; t) = \int_0^t \int_{\Omega} h |R_h(U, P)|^2 dxdt, \tag{11}$$

is an analog of  $D_\nu(u; t)$  with  $h \sim \nu$ , where  $R_h(U, P)$  is the Euler residual of  $(U, P)$ . We see that the G2 turbulent viscosity  $D_h(U; t)$  arises from penalization of a non-zero Euler residual  $R_h(U, P)$  with the penalty directly connecting to the violation (according the theory of criminology). A turbulent solution is characterized by substantial dissipation  $D_h(U; t)$  with  $\|R_h(U, P)\|_0 \sim h^{-1/2}$ , and

$$\|R_h(U, P)\|_{-1} \leq \sqrt{h} \tag{12}$$

in accordance with (8) and (9).

## 20 Wellposedness of Mean-Value Outputs

Let  $M(v) = \int_Q v\psi dxdt$  be a *mean-value output* of a velocity  $v$  defined by a smooth weight-function  $\psi(x, t)$ , and let  $(u, p)$  and  $(U, P)$  be two G2-solutions on two meshes with maximal mesh size  $h$ . Let  $(\varphi, \theta)$  be the solution to the *dual linearized problem*

$$\begin{aligned} -\dot{\varphi} - (u \cdot \nabla)\varphi + \nabla U^\top \varphi + \nabla \theta &= \psi && \text{in } \Omega \times I, \\ \nabla \cdot \varphi &= 0 && \text{in } \Omega \times I, \\ \varphi \cdot n &= g && \text{on } \Gamma \times I, \\ \varphi(\cdot, T) &= 0 && \text{in } \Omega, \end{aligned} \tag{13}$$

where  $\top$  denotes transpose. Multiplying the first equation by  $u - U$  and integrating by parts, we obtain the following output error representation [25]:

$$M(u) - M(U) = \int_Q (R_h(u, p) - R_h(U, P)) \cdot \varphi \, dxdt \quad (14)$$

where for simplicity the dissipative terms are here omitted, from which follows the a posteriori error estimate:

$$|M(u) - M(U)| \leq S(\|R_h(u, p)\|_{-1} + \|R_h(U, P)\|_{-1}), \quad (15)$$

where the stability factor

$$S = S(u, U, M) = S(u, U) = \|\varphi\|_{H^1(Q)}. \quad (16)$$

In [25] we present a variety of evidence, obtained by computational solution of the dual problem, that for global mean-value outputs such as drag and lift,  $S \ll 1/\sqrt{h}$ , while  $\|R_h\|_{-1} \sim \sqrt{h}$ , allowing computation of drag/lift with a posteriori error control of the output within a tolerance of a few percent. In short, mean-value outputs such as lift and drag are wellposed and thus physically meaningful.

We explain in [25] the crucial fact that  $S \ll 1/\sqrt{h}$ , heuristically as an effect of *cancellation* of rapidly oscillating reaction coefficients of turbulent solutions combined with smooth data in the dual problem for mean-value outputs. In smooth potential flow there is no cancellation, which explains why zero lift/drag cannot be observed in physical flows.

As an example, we show in Fig.8 turbulent G2 flow around a car with substantial drag in qualitative accordance with wind-tunnel experiments. We see a pattern of streamwise vorticity forming in the rear wake. We also see surface vorticity forming on the hood transversal to the main flow direction. We see similar features in the flow of air around a wing.

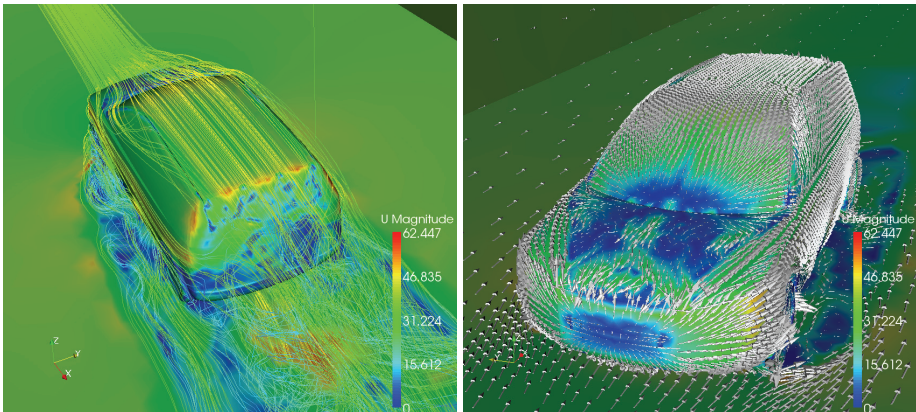


Figure 8: Velocity of turbulent G2 flow with slip around a car with courtesy of geometry Volvo Cars and computations by Murtazo Nasarov.

## 21 Scenario for Separation without Stagnation

We now present a scenario for transition of potential flow into turbulent flow, based on identifying perturbations of strong growth in the linearized equations (2) and (3) at separation generating rolls of low pressure streamwise vorticity changing the pressure distribution to give both lift and drag of a wing.

As a model of potential flow at rear separation, we consider the potential flow  $u(x) = (x_1, -x_2, 0)$  in the half-plane  $\{x_1 > 0\}$ . Assuming  $x_1$  and  $x_2$  are small, we approximate the  $v_2$ -equation of (2) by

$$\dot{v}_2 - v_2 = f_2,$$

where  $f_2 = f_2(x_3)$  is an oscillating mesh residual perturbation depending on  $x_3$  (including also a pressure-gradient), for example  $f_2(x_3) = h \sin(x_3/\delta)$ , with  $\delta > 0$ . It is natural to assume that the amplitude of  $f_2$  decreases with  $\delta$ . We conclude, assuming  $v_2(0, x) = 0$ , that

$$v_2(t, x_3) = t \exp(t) f_2(x_3),$$

and for the discussion, we assume  $v_3 = 0$ . Next we approximate the  $\omega_1$ -vorticity equation for  $x_2$  small and  $x_1 \geq \bar{x}_1 > 0$  with  $\bar{x}_1$  small, by

$$\dot{\omega}_1 + x_1 \frac{\partial \omega_1}{\partial x_1} - \omega_1 = 0,$$

with the “inflow boundary condition”

$$\omega_1(\bar{x}_1, x_2, x_3) = \frac{\partial v_2}{\partial x_3} = t \exp(t) \frac{\partial f_2}{\partial x_3}.$$

The equation for  $\omega_1$  thus exhibits exponential growth, which is combined with exponential growth of the “inflow condition”. We can see these features in Fig. 9 showing how opposing flows on the back generate a pattern of co-rotating surface vortices which act as initial conditions for vortex stretching into the fluid generating rolls of low-pressure streamwise vorticity, in the case of a wing attaching to the trailing edge.

Altogether we expect  $\exp(t)$  perturbation growth of residual perturbations of size  $h$ , resulting in a global change of the flow after time  $T \sim \log(1/h)$ , which can be traced in the computations.

We thus understand that the formation of streamwise streaks as the result of a force perturbation oscillating in the  $x_3$  direction, which in the retardation of the flow in the  $x_2$ -direction creates exponentially increasing vorticity in the  $x_1$ -direction, which acts as inflow to the  $\omega_1$ -vorticity equation with exponential growth by vortex stretching. Thus, we find exponential growth at rear separation in both the retardation in the  $x_2$ -direction and the acceleration in the  $x_1$  direction. This scenario is illustrated in principle and computation in Fig.9. Note that since the perturbation is convected with the base flow, the absolute size of the growth is related to the length of time the perturbation stays in a zone of exponential growth. Since the combined exponential growth is independent of  $\delta$ , it follows that large-scale perturbations with large amplitude have largest growth, which is also seen in computations with  $\delta$  the distance between streamwise rolls as seen in Fig.3 which does not seem to decrease with decreasing  $h$ .

Notice that at forward attachment of the flow the retardation does not come from opposing flows, and the zone of exponential growth of  $\omega_2$  is short, resulting in much smaller perturbation growth than at rear separation.

We can view the occurrence of the rear surface vorticities as a mechanism of separation with non-zero tangential speed, by diminishing the normal pressure gradient of potential flow, which allows separation only at stagnation. The surface vorticities thus allow separation without stagnation but the price is generation of a system of low-pressure tubes of streamwise vorticity creating drag in a form of “separation trauma” or “cost of divorce”.

The scenario for separation can be summarized as follows: Velocity instability in retardation as opposing flows meet in the rear of the cylinder, generates a zig-zag pattern of surface vorticity shown in Fig.9, allowing separation into counter-rotating low-pressure rolls, attaching to the trailing edge in the case of a wing, as shown in Fig. 1.

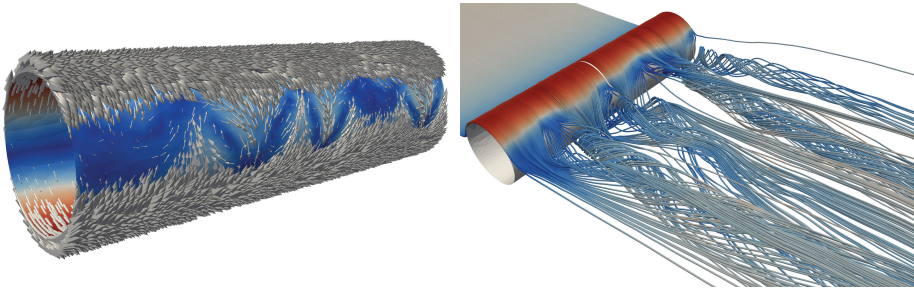


Figure 9: Turbulent separation by surface vorticity forming counter-rotating low-pressure rolls in flow around a circular cylinder, illustrating separation at the trailing edge of a wing [23].

## 22 Stability of the Streamwise Vorticity Perturbed Flow

The rolls of streamwise vorticity swirling flow appearing at separation because of the instability of potential flow represent a more stable flow pattern. An indication of stability is given by an analysis of the stability of the rotating flow field  $u = (0, x_3, -x_2)$  with linearized problem of the form

$$\dot{v}_2 + v_3 = 0, \quad \dot{v}_3 - v_2 = 0 \quad (17)$$

which does not have any exponentially unstable solutions. The swirling flow at separation is similar to the vortex seen at the drain of a bathtub.

## 23 Sailing

Both the sail and keel of a sailing boat under tacking against the wind, act like wings generating lift and drag, but the action, geometrical shape and angle of attack of the sail and the keel are different. The effective angle of attack of a sail is typically 15-20 degrees and that of a keel 5-10 degrees, for reasons which we now give.

The boat is pulled forward by the sail, assuming for simplicity that the beam is parallel to the direction of the boat at a minimal tacking angle, by the component  $L \sin(15)$  of the lift  $L$ , as above assumed to be perpendicular to the effective wind direction, but also by the following contributions from the drag assumed to be parallel to the effective wind direction: The negative drag on the leeward side at the leading edge close to the mast gives a positive pull which largely compensates for the positive drag from the rear leeward side, while there is less positive drag from the windward side of the sail as compared to a wing profile, because of the difference in shape. The result is a forward pull  $\approx \sin(15)L \approx 0.2L$  combined with a side (heeling) force  $\approx L \cos(15) \approx L$ , which tilts the boat and needs to be balanced by lift from the keel in the opposite direction. Assuming the lift/drag ratio for the keel is 13, the forward pull is then reduced to  $\approx (0.2 - 1/13)L \approx 0.1L$ , which can be used to overcome the drag from the hull minus the keel.

The shape of a sail is different from that of a wing which gives smaller drag from the windward side and thus improved forward pull, while the keel has the shape of a symmetrical wing and acts like a wing. A sail with aoa 15–20 degrees gives maximal pull forward at maximal heeling/lift with contribution also from the rear part of the sail, like for a wing just before stall, while the drag is smaller than for a wing at 15–20 degrees aoa (for which the lift/drag ratio is 4–3), with the motivation given above. The lift/drag curve for a sail is thus different from that of wing with lift/drag ratio at aoa 15–20 much larger for a sail. On the other hand, a keel with aoa 5–10 degrees has a lift/drag ratio about 13. A sail at aoa 15–20 thus gives maximal pull at strong heeling force and small drag, which together with a keel at aoa 5–10 with strong lift and small drag, makes an efficient combination. This explains why modern designs combine a deep narrow keel acting efficiently for small aoa, with a broader sail acting efficiently at a larger aoa.

Using a symmetrical wing as a sail would be inefficient, since the lift/drag ratio is poor at maximal lift at aoa 15–20. On the other hand, using a sail as a wing can only be efficient at a large angle of attack, and thus is not suitable for cruising. This material is developed in more detail in [30].

## References

- [1] How Airplanes Fly: A Physical Description of Lift, <http://www.allstar.fiu.edu/aero/airfly/v13.htm>.
- [2] J. D. Anderson, *A History of Aerodynamics*, Cambridge Aerospace Series 8, Cambridge University Press, 1997.
- [3] <http://www.aviation-history.com/theory/lift.htm>
- [4] AVweb, <http://www.avweb.com/news/airman/183261-1.html>.
- [5] Y. Bazilevs, C. Michler, V.M. Calo and T.J.R. Hughes, Turbulence without Tears: Residual-Based VMS, Weak Boundary Conditions, and Isogeometric Analysis of Wall-Bounded Flows, Preprint 2008.
- [6] W. Beaty, Airfoil Lifting Force Misconception Widespread in K-6 Textbooks, Science Hobbyist, <http://www.eskimo.com/billb/wing/airfoil.htm#L1>.
- [7] Garret Birkhoff, *Hydrodynamics: a study in logic, fact and similitude*, Princeton University Press, 1950.

- [8] K. Chang, Staying Aloft; What Does Keep Them Up There?, New York Times, Dec 9, 2003.
- [9] S. Cowley, Laminar boundary layer theory: A 20th century paradox, Proceedings of ICTAM 2000, eds. H. Aref and J.W. Phillips, 389-411, Kluwer (2001).
- [10] G. M. Craig, Stop Abusing Bernoulli! - How Airplanes Really Fly, Regenerative Press, 1998.
- [11] A. Crook, Skin friction estimation at high Reynolds numbers and Reynolds-number effects for transport aircraft, Center for Turbulence Research, 2002.
- [12] D'Alembert's paradox, [en.wikipedia.org/wiki/D'Alembert's\\_paradox](http://en.wikipedia.org/wiki/D'Alembert's_paradox).
- [13] 3rd CFD AIAA Drag Prediction Workshop, [aac.larc.nasa.gov/tfcab/cfdlarc/aiaa-dpw](http://aac.larc.nasa.gov/tfcab/cfdlarc/aiaa-dpw).
- [14] O. Darrigol, World of Flow, A History of hydrodynamics from the Bernoullis to Prandtl, Oxford University Press.
- [15] J. Hadamard, Sur les problÃ©mes aux dÃ©rivÃ©es partielles et leur signification physique, Princeton University Bulletin, 49-52, 1902.
- [16] A. Fage and L.F. Simmons, An investigation of the air-flow pattern in the wake of an airfoil of finite span, Rep.Memor.aero.REs.Coun.,Lond.951, 1925.
- [17] The FEniCS Project, [www.fenics.org](http://www.fenics.org).
- [18] U. Frisch, Turbulence: The Legacy of A. N. Kolmogorov. Cambridge University Press, 1995.
- [19] S. Goldstein, Fluid mechanics in the first half of this century, in Annual Review of Fluid Mechanics, Vol 1, ed. W. R. Sears and M. Van Dyke, pp 1-28, Palo Alto, CA: Annua Reviews Inc.
- [20] N. Gregory and C.L. O'Reilly, Low-Speed Aerodynamic Characteristics of NACA 0012 Aerofoil Section, including the Effects of Upper-Surface Roughness Simulating Hoar Frost, Aeronautical Research Council Reports and Memoranda, <http://aerade.cranfield.ac.uk/ara/arc/rm/3726.pdf>.
- [21] J.Hoffman, Simulation of turbulent flow past bluff bodies on coarse meshes using General Galerkin methods: drag crisis and turbulent Euler solutions, Comp. Mech. 38 pp.390-402, 2006.
- [22] J. Hoffman, Simulating Drag Crisis for a Sphere using Friction Boundary Conditions, Proc. ECCOMAS, 2006.
- [23] J.Hoffman and Niclas Jansson, A computational study of turbulent flow separation for a circular cylinder using skin friction boundary conditions, Proc. Quality and Reliability of Large Eddy Simulation, Pisa, 2009.
- [24] J. Hoffman and C. Johnson, Blowup of Euler solutions, BIT Numerical Mathematics, Vol 48, No 2, 285-307.
- [25] J. Hoffman and C. Johnson, *Computational Turbulent Incompressible Flow*, Springer, 2007, [www.bodysoulmath.org/books](http://www.bodysoulmath.org/books).
- [26] J. Hoffman and C. Johnson, Resolution of d'Alembert's paradox, Journal of Mathematical Fluid Mechanics, Online First, Dec 10, 2008.
- [27] J. Hoffman and C. Johnson, Separation in slightly viscous flow, to appear.
- [28] J. Hoffman and C. Johnson, Is the Clay Navier-Stokes Problem Wellposed?, NADA 2008, <http://www.nada.kth.se/~cgjoh/hadamard.pdf>, <http://knol.google.com/k/the-clay-navier-stokes-millennium-problem>.

- [29] J. Hoffman and C. Johnson, The Secret of Flight, <http://www.nada.kth.se/~cgjoh/ambsflying.pdf>
- [30] J. Hoffman and C. Johnson, The Secret of Sailing, <http://www.nada.kth.se/~cgjoh/ambssailing.pdf>
- [31] J. Hoffman and C. Johnson, Movies of take-off of Naca0012 wing, <http://www.csc.kth.se/ctl>
- [32] <http://knol.google.com/k/claes-johnson/dalemberts-paradox/yvfu3xg7d7wt/2>.
- [33] <http://knol.google.com/k/claes-johnson/why-it-is-possible-to-fly/yvfu3xg7d7wt/18>.
- [34] HowStuffWorks, <http://science.howstuffworks.com/airplane7.htm>.
- [35] G.S. Jones, J.C. Lin, B.G. Allan, W.E. Milholen, C.L. Rumsey, R.C. Swanson, Overview of CFD Validation Experiments for Circulation Control Applications at NASA.
- [36] R. Kunzig, An old, lofty theory of how airplanes fly loses some altitude, *Discover*, Vol. 22 No. 04, April 2001.
- [37] F. W. Lanchester, *Aerodynamics*, 1907.
- [38] Experiments in Aerodynamics, Smithsonian Contributions to Knowledge no. 801, Washinton, DC, Smithsonian Institution.
- [39] W. Layton, Weak imposition of no-slip boundary conditions in finite element methods, *Computers and Mathematics with Applications*, 38 (1999), pp. 129–142.
- [40] W. J. McCroskey, A Critical Assessment of Wind Tunnel Results for the NACA 0012 Airfoil, NASA Technical Memorandum 10001, Technical Report 87-A-5, Aeroflightdynamics Directorate, U.S. Army Aviation Research and Technology Activity, Ames Research Center, Moffett Field, California.
- [41] <http://web.mit.edu/16.00/www/aec/flight.html>.
- [42] P. Moin and J. Kim, Tackling Turbulence with Supercomputers, *Scientific American Magazine*, 1997.
- [43] <http://www.grc.nasa.gov/WWW/K-12/airplane/lift1.html>.
- [44] <http://www.planeandpilotmag.com/aircraft/specifications/diamond/2007-diamond-star-da40-xl/289.html>
- [45] L. Prandtl, On Motion of Fluids with Very Little, in *Verhandlungen des dritten internationalen Mathematiker-Kongresses in Heidelberg 1904*, A. Krazer, ed., Teubner, Leipzig, Germany (1905), p. 484. English trans. in *Early Developments of Modern Aerodynamics*, J. A. K. Ackroyd, B.P. Axcell, A.I. Ruban, eds., Butterworth-Heinemann, Oxford, UK (2001), p. 77.
- [46] L. Prandtl and O Tietjens, *Applied Hydro- and Aeromechanics*, 1934.
- [47] H. Schlichting, *Boundary Layer Theory*, McGraw-Hill, 1979.
- [48] K. Stewartson, D’Alembert’s Paradox, *SIAM Review*, Vol. 23, No. 3, 308-343. Jul., 1981.
- [49] B. Thwaites (ed), *Incompressible Aerodynamics*, An Account of the Theory and Observation of the Steady Flow of Incompressible Fluid pas Aerofoils, Wings and other Bodies, Fluid Motions Memoirs, Clarendon Press, Oxford 1960, Dover 1987, p 94.
- [50] R. von Mises, *Theory of Flight*, McGraw-Hill, 1945.
- [51] D. You and P. Moin, Large eddy simulation of separation over an airfoil with synthetic jet control, Center for Turbulence Research, 2006.